Exp Brain Res (2016) 234:2747–2760
DOI 10.1007/s00221-016-4725-2

RESEARCH ARTICLE

Imidazoleacetic acid-ribotide in vestibulo-sympathetic pathway neurons

Gay R. Holstein[1,2,3] · **Victor L. Friedrich Jr.**[2] · **Giorgio P. Martinelli**[1]

Received: 31 May 2016 / Accepted: 6 July 2016 / Published online: 13 July 2016

Abstract Imidazole-4-acetic acid-ribotide (IAARP) is a putative neurotransmitter/modulator and an endogenous regulator of sympathetic drive, notably systemic blood pressure, through binding to imidazoline receptors. IAARP is present in neurons and processes throughout the CNS, but is particularly prevalent in regions that are involved in blood pressure control. The goal of this study was to determine whether IAARP is present in neurons in the caudal vestibular nuclei that participate in the vestibulo-sympathetic reflex (VSR) pathway. This pathway is important in modulating blood pressure upon changes in head position with regard to gravity, as occurs when humans rise from a supine position and when quadrupeds climb or rear. Sinusoidal galvanic vestibular stimulation was used to activate the VSR and *cfos* gene expression in VSR pathway neurons of rats. These subjects had previously received a unilateral FluoroGold tracer injection in the rostral or caudal ventrolateral medullary region. The tracer was transported retrogradely and filled vestibular neuronal somata with direct projections to the injected region. Brainstem sections through the caudal vestibular nuclei were immunostained to visualize FluoroGold, cFos protein, IAARP and glutamate immunofluorescence. The results demonstrate that IAARP is present in vestibular neurons of the VSR pathway, where it often co-localizes with intense glutamate immunofluorescence. The co-localization of IAARP and intense glutamate immunofluorescence in VSR neurons may represent an efficient chemoanatomical configuration, allowing the vestibular system to rapidly up- and down-modulate the activity of presympathetic neurons in the ventrolateral medulla, thereby altering blood pressure.

Keywords Vestibular · Blood pressure · Otolith · Sympathetic nerve activity · Galvanic vestibular stimulation

Introduction

The semicircular canals and otolith organs detect angular and linear accelerations impinging on the head, respectively, and convey that information to the vestibular nuclei in the brainstem. The vestibular nuclei, in turn, give rise to effector pathways that participate in the control of eye movements, posture, balance, and some aspects of autonomic function (Vidal et al. 2015). The latter projections inform central presympathetic autonomic nervous system neurons influencing blood pressure, respiration and gastrointestinal activity about changes in posture, and body position with regard to gravity. Collectively, these functional pathways are referred to as the vestibulo-sympathetic reflex (VSR) (Yates et al. 2014).

One component of the VSR is a direct projection from the caudal vestibular nuclei to the rostral ventrolateral medulla (RVLM) (Holstein et al. 2011a), a region that contains the C1 adrenergic cell group as well as non-C1 presympathetic neurons (Ruggiero et al. 1994; Lipski et al. 1995; Schreihofer and Guyenet 1997). The RVLM is an important site of action of anti-hypertensive drugs such as

✉ Gay R. Holstein
gay.holstein@mssm.edu

[1] Department of Neurology, Icahn School of Medicine at Mount Sinai, Box 1140, One Gustave L. Levy Place, New York, NY 10029, USA

[2] Department of Neuroscience, Icahn School of Medicine at Mount Sinai, New York, NY, USA

[3] Department of Anatomy/Functional Morphology, Icahn School of Medicine at Mount Sinai, New York, NY, USA

clonidine, moxonidine and rilmenidine (Ernsberger et al. 1993; Regunathan and Reis 1996; Eglen et al. 1998) that bind to imidazoline receptors (IRs) and/or α_2 adrenergic receptors in the region. While both C1 and non-C1 bulbospinal neurons may have a role in the medullary circuits regulating blood pressure, the rapid excitatory pathway from RVLM to spinal cord sympathetic preganglionic neurons appears to be mediated by glutamate (Deuchars et al. 1995) (reviews: Morrison 2003; Stornetta 2009).

Areas of the vestibular nuclei also project to the caudal ventrolateral medulla (CVLM), a region that participates in baroreflex-mediated modulation of blood pressure. CVLM receives baroreceptor-related inputs from the solitary nucleus and supplies both excitatory and GABAergic inhibitory projections to RVLM. We have previously demonstrated that the VSR pathways to RVLM and CVLM are activated by sinusoidal galvanic vestibular stimulation (sGVS) (Holstein et al. 2012), causing alterations in blood pressure (Cohen et al. 2013). Many of the vestibular nuclear neurons that are activated by this vestibular stimulus and that project to RVLM and/or CVLM display intense glutamate immunofluorescence (Holstein et al. 2016).

Imidazole-4-acetic acid-ribotide (IAARP) is a putative neurotransmitter/modulator in the CNS and an endogenous IR agonist (Prell et al. 2004). It is an intrinsic regulator of sympathetic drive, notably systemic blood pressure. IAARP is present in some central vestibular neurons (Martinelli et al. 2007) and in scattered cells throughout the CNS (Friedrich et al. 2007), including the RVLM (Holstein et al. 2011b). In the hippocampus, IAARP suppresses excitatory glutamatergic synaptic transmission at Schaffer collateral synapses with CA1 pyramidal cells (Bozdagi et al. 2011), and this inhibition includes both pre-and postsynaptic IR-mediated effects.

The goal of the present study was to determine whether vestibular neurons that participate in the VSR contain IAARP. Multiple-label immunofluorescence staining was conducted to identify IAARP in vestibular neurons that accumulated cFos protein in response to sGVS activation in animals that had received retrograde tracer injections in RVLM or CVLM. The additional goal of this study was to assess the co-localization of IAARP with intense glutamate immunofluorescence in VSR pathway neurons. The results demonstrate that IAARP is present in vestibular nucleus neurons of the VSR pathway, where it partially but not exclusively co-localizes with intense glutamate immunofluorescence.

Methods

Subjects

All experiments were conducted in accordance with the NRC Guide for the Care and Use of Laboratory Animals (8th Edition 2011) and were approved by the Institutional Care and Use Committee of the Icahn School of Medicine at Mount Sinai. Data were obtained from 14 adult male Long-Evans rats (Harlan Laboratories, MA) weighing 350–450 g. Seven of these animals received injections of the retrograde tracer FluoroGold (Fluorochrome, LLC, Denver, CO) in RVLM, five had FluoroGold injections in CVLM, and two received vestibular stimulation but no tracer injection. Sections from many (but not all) of these rats have been used in several of our previous studies (Holstein et al. 2014, 2016).

Retrograde tracer injections

FluoroGold was utilized because of its high sensitivity, low probability of uptake by fibers of passage, and lack of concomitant anterograde transport (Raju and Smith 2006; Schofield 2008). As previously described (Holstein et al. 2014, 2016), rats were anesthetized with isoflurane (4 % induction, 2 % maintenance), shaved and then placed in a computer-assisted stereotaxic frame (Leica *Angle Two*, Leica Microsystems, St. Louis, MO). Body temperature was maintained by laying the animal on a homeothermic pad regulated by feedback from a rectal thermometer. Ophthalmic ointment kept the eyes moist, and a single dose of analgesic (Buprenex, 0.05 mg/kg, SQ; Reckitt Benckiser Pharmaceuticals; Richmond VA) was administered preemptively. After draping for aseptic surgery, the head and neck were disinfected with Povidone. A midline incision was made from the top of the skull to the C1 vertebra, and the atlanto-occipital membrane was exposed. A glass pipette (tip OD 20–25 μm) filled with 2 % FluoroGold dissolved in saline was mounted on the *Angle Two* dorsoventral (DV) drive tilted 45° above the horizontal plane. The pipette tip was positioned at Bregma, and the target coordinates for RVLM (ML ± 2.34; AP −12.24; DV −10.21) or CVLM (ML ± 2.2; AP −12.80; DV −10.0) (Paxinos and Watson 2009) were entered in the computer. The *Angle Two* AP and ML drives were then adjusted, and the pipette was advanced under computer guidance toward the brainstem target via a small (~2 mm dia.) burr hole drilled at ML ± 2.3 mm. The tracer solution was iontophoresed at +5 μA for 10 min (7 s on, 7 s off), and the pipette was left in place for 2–3 min after the iontophoresis, before being slowly withdrawn. The neck muscles were sutured, and the skin was closed with surgical clips. Rats received 3–4 ml of sterile saline SQ at the end of the procedure. Analgesics were administered twice daily for 3 days after surgery (Buprenex; 0.05 mg/kg; SQ), and the animals were allowed to recover for 10–14 days before the terminal experiment was performed. The rats recovered fully, and we did not observe postoperative head tilt, body tilt, or locomotor activity favoring the unoperated side.

sGVS

Animals were anesthetized with isoflurane (4 % induction; 2 % maintenance) and maintained on a homeothermic pad. Ag/AgCl needle electrodes (BAK) connected to a computer-controlled current stimulator (Holstein et al. 2012) were inserted bilaterally under the skin over the mastoid processes. An individual sGVS stimulus comprised 5 cycles of binaural current (2 mA, 0.025 Hz). This stimulus was repeated 5 times with 3 min between repetitions. Rats were then allowed to recover from the anesthesia and were euthanized 90 min after the cessation of the last sGVS stimulus.

Tissue harvesting and processing

Perfusion, fixation, and tissue sectioning

Rats were anesthetized with isoflurane (as above) and then perfused transcardially 90 min after the sGVS stimulation, a time point of significant cFos protein accumulation in vestibular neurons after sGVS or tilt (Holstein et al. 2012, 2014). The initial perfusion with 100 ml of 37 °C 10 mM phosphate buffered saline (PBS) was followed by 500 ml of 4 % paraformaldehyde/0.2 % glutaraldehyde fixative in 0.1 M PB (pH 7.4) at room temperature. Brains were harvested immediately after perfusion, cut into blocks using an adult rat brain coronal matrix (Ted Pella, Inc.; Redding, CA), and stored at 4 °C in PBS with 0.02 % NaN_3. The block containing the vestibular nuclear complex and ventrolateral medullary region was cut by vibrating microtome into 50 µm serial sections (~120 per animal) that were stored at 4 °C in PBS containing 0.02 % NaN_3.

Anatomical localization

The locations of the four principal vestibular nuclei were determined in each tissue section by comparing the anatomical landmarks on the dorsal aspect of the tissue with a standard stereotaxic atlas (Paxinos and Watson 2005). Although this atlas was made using sections from Wistar rats, and the present study utilized the Long-Evans strain, we did not observe any significant neuroanatomical differences in the caudal vestibular nuclei, RVLM, or CVLM of the two strains. Moreover, the *Angle Two* injection guidance system utilizes Paxinos and Watson coordinates, and our success rate in targeting the structures of interest is ~80 %. This suggests that the Paxinos and Watson stereotaxic atlas coordinates are sufficient for the level of resolution required in this study.

The boundaries of RVLM and CVLM were determined by comparing the structures on the ventral aspect of the tissue sections with published maps and atlases of those regions (Paxinos and Watson 2005, 2009; Card et al. 2006; Bourassa et al. 2009; Goodchild and Moon 2009). Based on the most conservative estimates from these maps, RVLM was identified as a 1 mm rostrocaudal region extending from approximately 11.8–12.8 mm caudal to Bregma. The other dimensions of RVLM were determined by a triangle with nucleus ambiguus (pars compacta) at the apex and the ventral aspect of the medulla 1.4 and 2.2 mm lateral to the midline as the other two points. The CVLM region, located 12.8–13.6 mm caudal to Bregma, was similarly defined according to anatomical coordinates. Both regions correspond well with functional and physiological maps of RVLM and CVLM (Goodchild and Moon 2009). The locations of RVLM and CVLM were further verified in our experimental animals using tyrosine hydroxylase and GABA immunostaining of representative sections through these regions (Holstein et al. 2011a).

Primary antibodies

Individual tissue sections were immunostained using one of the following primary antibody combinations: (1) anti-FluoroGold and anti-IAARP; (2) anti-FluoroGold, anti-IAARP, and anti-cFos; (3) anti-FluoroGold, anti-IAARP, and anti-glutamate; and (4) anti-FluoroGold, anti-IAARP, anti-glutamate, and anti-cFos. Antibody sources and descriptions are shown in Table 1. The rationale for their use, staining protocols, and controls are described below.

In previous studies, we assessed several commercial antibodies against cFos including two unconjugated rabbit polyclonal antisera (Santa Cruz Biotechnology, Cat.#

Table 1 Primary antibodies used in this study

Antigen	Host and type	Immunogen	Source	Working dilutions
FluoroGold	Rabbit polyclonal	FluoroGold	Millipore; Cat. # AB153	1:400 (IMF); 1:5000 (DAB)
cFos	Rabbit polyclonal	A peptide mapping within an internal region of human cFos	Santa Cruz Biotech; Cat. # sc-253	1:500
Glutamate	Mouse monoclonal	Glutamate-glutaraldehyde-BSA conjugate	Our laboratory	1:10
IAARP	Rabbit polyclonal	I-AA-RP-KLH conjugate	Our laboratory	1:500

sc-253; Calbiochem, Cat.# PC38) and one rabbit polyclonal antiserum directly conjugated with AlexaFluor 488 (Santa Cruz Biotechnology, Cat. # sc-253 AF488) (Holstein et al. 2012). Although the three reagents stained the same vestibular regions and cell types, the unlabeled polyclonal sera provided more robust labeling in multiple-label immunofluorescence experiments. To assess non-specific staining, control tissue sections were exposed to a mixture of the rabbit polyclonal antibody preabsorbed with blocking peptide (Santa Cruz Biotechnology; Cat.# sc-253P); no immunolabeling was apparent in these sections. Previous studies in our laboratory have demonstrated that cFos-peroxidase immunolabeling in mock (non)-sGVS-stimulated rats comprises less than three neurons/vestibular region/tissue section (Holstein et al. 2012). Given the higher sensitivity of the peroxidase labeling system, fewer non-stimulation-dependent cFos-positive vestibular neurons are likely to be obtained using the immunofluorescence approach taken in the present study.

The FluoroGold tracer was amplified by immunostaining with a rabbit polyclonal anti-FluoroGold serum (Millipore; Cat.# AB153). Both the cFos and FluoroGold primary antibodies provided staining of the same vestibular regions and cells observed previously (Holstein et al. 2012, 2014, 2016).

The anti-IAARP sera were raised in rabbits immunized with an I-4-AA-RP-keyhole limpet hemocyanin conjugate (Prell et al. 2004). The production, characterization, and binding specificity of this antibody have been described in detail previously (Prell et al. 2004; Friedrich et al. 2007; Martinelli et al. 2007). The mouse IgG1 monoclonal anti-glutamate antibody was also produced in our laboratory. The complete description of the production, characterization, and specificity of this antibody was previously published (Holstein et al. 2004). Subsequently, we performed additional assays to verify (i) that glutamate can be fixed in situ by glutaraldehyde and (ii) that paraformaldehyde/glutaraldehyde-fixed glutamate can specifically be recognized by the monoclonal antibody (MAb 215B2) used in the present study (Holstein et al. 2011a).

Peroxidase/diaminobenzidine immunocytochemistry

To identify the FluoroGold injection sites in the RVLM or CVLM, regularly spaced vibratome sections (250 µm apart) from each injected rat were incubated in blocking buffer (PBS with 10 % normal goat serum, 0.02 % NaN_3, and 0.1 % Triton X-100) for 4–6 h or overnight, and then in anti-FluoroGold antibody (1:5000 in blocking buffer) for 12–18 h. After thorough rinsing (6 changes of PBS over 4–6 h), the free-floating sections were incubated in peroxidase-conjugated goat anti-rabbit secondary antibody (Jackson ImmunoResearch Cat. # 111-035-144; 1:2000 in blocking buffer without NaN_3) overnight. Sections were then rinsed in PBS (6 changes over 2 h) and incubated in diaminobenzidine (DAB; 0.5 mg/ml; Sigma D-5905; St. Louis, MO) diluted in 0.1 M Tris buffer (pH 7.6) with 0.01 % H_2O_2 for 5–10 min at room temperature. The reaction was stopped by repeated PBS rinses. Control sections were processed concomitantly and were treated as above except for the omission of primary and/or secondary antibodies (two sections per rat per control condition; 6 DAB control sections per rat).

Immunofluorescence

Tissue sections were processed for multiple-label immunofluorescence detection of combinations of primary and secondary reagents. Some sections were also stained with DAPI (ThermoFisher Scientific; Cat # D-1306) to visualize the location and approximate size range of cell nuclei (data not shown). Since the cFos, FluoroGold, and IAARP primary antibodies were raised in rabbit, the studies were performed by sequential application of primary and secondary antibodies. Briefly: (i) sections were exposed initially to rabbit anti-cFos primary followed by fluorochrome-labeled (e.g., DyLight 649) Fab fragment of a goat anti-rabbit IgG secondary, (ii) unreacted sites on the anti-cFos were blocked using a high concentration of *unlabeled* Fab fragment of goat anti-rabbit secondary antibody, (iii) stained sections were exposed to rabbit anti-FluoroGold followed by goat anti-rabbit IgG secondary antibody tagged with a different fluorochrome (e.g., DyLight 594), (iv) unreacted sites were blocked as above, and (v) the stained sections were exposed to rabbit anti-IAARP followed by goat anti-rabbit IgG secondary antibody tagged with a third fluorochrome (e.g., AlexaFluor 488). The sequence of primaries was varied across staining experiments, and each sequence was utilized in multiple tissue sections from each animal. An example of the overall staining procedure is provided below.

Example staining procedure: All steps were performed at room temperature with agitation on an orbital shaker. Free-floating sections were immersed in blocking buffer (3–6 h); incubated in rabbit anti-cFos primary antibody (1:500 in blocking buffer; 12–18 h); rinsed with multiple changes of PBS (4–8 h); incubated in AlexaFluor- or DyLight-conjugated goat anti-rabbit IgG (H + L) antibody Fab fragment (8 µg/ml in blocking buffer; Jackson ImmunoResearch; 12–18 h); rinsed in multiple changes of PBS (4–8 h); fixed with 2 % paraformaldehyde (10 min); rinsed (as above); incubated in unlabeled Fab fragment goat anti-rabbit IgG (20 µg/ml in blocking buffer; Jackson ImmunoResearch; 12–18 h); rinsed; incubated in a mixture of rabbit anti-FluoroGold primary antibody (1:400 in blocking buffer) and mouse anti-glutamate (1:10 hybridoma supernatant

in blocking buffer) for 12–18 h; rinsed; and immersed in AlexaFluor-conjugated goat anti-rabbit IgG (H + L) (1:400 in blocking buffer; Invitrogen), and AlexaFluor-conjugated goat anti-mouse IgG (H + L) (1:300 in blocking buffer; Invitrogen). Following this staining, sections were incubated in DAPI solution (300 nM in PBS; 30 min). After final washes, all sections were mounted on glass slides and coverslipped using Prolong Gold antifade mounting medium (Invitrogen). Because different secondary antibodies have different degrees of sensitivity, various secondary antibodies and several alternative fluorochromes (in different sections) were used to detect each primary antibody.

Multiple staining controls were included in each experiment. To control for non-specific secondary antibody staining, sections were labeled with multiple secondary antibodies but no primary antibody. To control for secondary antibody cross-reactivity, tissue sections from each rat were labeled with multiple secondary antibodies but only one primary antibody. Lastly, to control for tissue autofluorescence, sections were treated with the blocking and rinsing steps, but no primary or secondary antibody incubations. All data for this study derived from experiments in which each secondary antibody bound exclusively to its appropriate primary antibody, and there was no binding to the inappropriate primary reagents. Importantly, all of the immunofluorescence-stained sections contained profiles that were stained by only one of the colors in the specimen's secondaries mixture (see Figures). This provided further assurance within each individual section that only one secondary antibody bound to each primary antibody, and therefore that secondary antibody cross-reactivity was insignificant.

Microscopy and figure preparation

Sections were examined and imaged using a Zeiss Axioplan2 microscope equipped with structured illumination (ApoTome). Each session included images of intensity-calibrated fluorescent beads (InSpeck, ThermoFisher), which allowed the intensity values in the images to be transformed to a scale based on the beads and therefore reasonably independent of image recording conditions. This strategy is advantageous because it permits comparisons of fluorescence intensities across specimens, experiments, and imaging sessions. Using this approach, the level of fluorescence designated as "intense" was set at 75 % of maximal fluorescence intensity.

Immunofluorescence was recorded using multichannel gray scale single slices and z-stacks. The images were analyzed by assessing the immunofluorescence present in each gray scale optical slice of each single channel separately. For z-stack images, antibody co-localization was initially screened using maximum intensity projections through the z-stacks, and both x–z and y–z side views of pseudocolored image stacks constructed using the Zeiss ApoTome software. Co-localization was then verified by comparing the gray scale immunofluorescence present in each individual channel within the same optical slice. Volocity, ImageJ and AxioVision were used to generate z-axis maximum intensity projections of whole stacks or selected subsets of optical sections for presentation figures. Figures were prepared (cropped, sized, colored, labeled, annotated) using Adobe Photoshop and Illustrator CC2015. Adjustments of brightness and contrast were performed using the Photoshop levels and curves tools applied to all parts of each image. The details of our image processing strategy for figure preparation, albeit with earlier versions of the same software, are published in (Holstein et al. 2014).

Results

Unilateral FluoroGold injections into RVLM ($N = 7$) and CVLM ($N = 5$) were performed 10–14 days prior to euthanasia. This provided sufficient time for the tracer to be transported retrogradely to the cell bodies of vestibular nuclear neurons. After tissue sectioning, the injection sites and diffusion penumbrae were visualized in regularly spaced sections (one every 250 μm) through the ventrolateral medulla stained for FluoroGold immunocytochemistry. The rostrocaudal extent of the tracer in each rat used in the present study is presented in Table 2. In general, the injection sites and surrounding penumbrae extended less than 1 mm medio-laterally and less than 750 μm dorso-ventrally.

Table 2 FluoroGold injection sites

	Caudal	Center	Rostral
RVLM			
R600	−12.60	−12.30	−12.00
R652	−12.80	−12.40	−11.88
R687	−12.28	−11.90	−11.78
R696	−12.57	−12.11	−11.88
R698	−12.66	−12.43	−12.12
R700	−12.60	−12.36	−12.18
R701A	−12.84	−12.36	−12.12
CVLM			
R608	−13.36	−13.08	−12.88
R688	−13.66	−13.41	−13.16
R690	−13.68	−13.43	−12.93
R695	−13.56	−13.22	−12.30
R697	−13.44	−13.20	−12.96

Legend approximate Bregma levels of the tracer injection site (center) and the rostral and caudal extent of the diffusion penumbra in RVLM or CVLM of all rats used in this study

Additional sets of transverse sections through the vestibular nuclei from animals with verified tracer injections were then double labeled with anti-FluoroGold and anti-IAARP. Double-labeled neurons were observed in the caudal half of the medial and spinal vestibular nuclei (MVN and SpVN, respectively), but not more rostrally and not in magnocellular MVN. Although double-labeled neurons were present bilaterally, they were more prevalent in vestibular nuclei ipsilateral to the injection site. Three cytological types of FluoroGold-filled and IAARP-immunofluorescent neurons were observed: small fusiform neurons, larger multipolar cells, and small spherical neurons (Fig. 1).

The presence of FluoroGold in vestibular cell bodies was interpreted as evidence that the tracer-filled neurons sent axonal projections to the ventrolateral medulla. To verify that such cells participate in the functional VSR, low frequency binaural sGVS was used to stimulate vestibular afferent nerve fibers in the rats prior to euthanasia. Activation of central vestibular neurons was then assessed by immunofluorescence detection of cFos protein (Holstein et al. 2012). Tissue sections from the tracer-injected rats were immunostained concomitantly for cFos, FluoroGold, and IAARP. We found that IAARP was present in sGVS-activated vestibulo-sympathetic projection neurons, as well as in vestibular neurons that were not tracer-filled and/or did not accumulate cFos protein after sGVS (Fig. 2). The activated (cFos+) VN neurons that contain IAARP but *not* FluoroGold (e.g., Fig 3b) are interpreted as vestibular neurons with projections exclusively to the contralateral R/CVLM, or VSR cells with projections to the ipsilateral side, but to the non-injected VLM subregion (CVLM or RVLM). In both circumstances, cFos activation is expected, but retrograde tracer is not. Triple-labeled cells of all three cytologic types were observed in both SpVN and MVN, projecting to RVLM and CVLM (Fig. 3).

We have previously reported that many sGVS-activated vestibular neurons with projections to CVLM or RVLM are intensely glutamate immunofluorescent (Holstein et al. 2016). To determine whether IAARP is co-localized in these neurons, sections from FluoroGold-injected rats were immunostained to visualize the tracer together with IAARP and glutamate. The low-affinity monoclonal anti-glutamate antibody used in this study has previously been described in detail (Holstein et al. 2004, 2011a). While some neurons had barely detectable immunofluorescence signal, presumably reflecting the metabolic role of glutamate in cells, a subset of neurons were intensely immunofluorescent. Only these latter cells were designated as glutamate-immunofluorescent neurons in the present study (see "Methods" section). We observed that many, but not all, of the neurons that co-localized tracer and IAARP were glutamate immunofluorescent (Fig. 4). All three cytological types of neurons that were previously identified by retrograde tracing

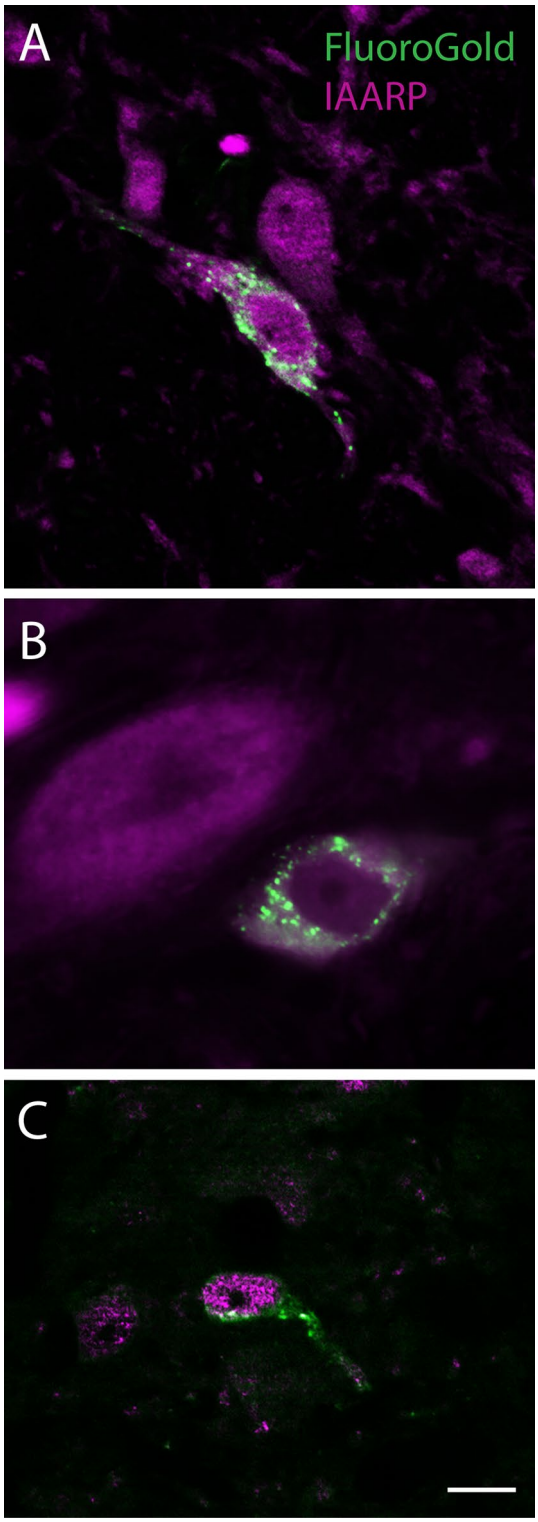

Fig. 1 Examples of the three types of FluoroGold-labeled neurons (punctate label) that co-localize IAARP. **a** A fusiform neuron in SpVN that was retrogradely filled with tracer after an injection in ipsilateral RVLM. **b** A larger diameter neuron in caudal MVN that was double labeled after an injection in ipsilateral CVLM. **c** A small spherical neuron in the MVN that was double labeled after a tracer injection into the contralateral RVLM. *Scale bar* in C is 10 μm in all *panels*

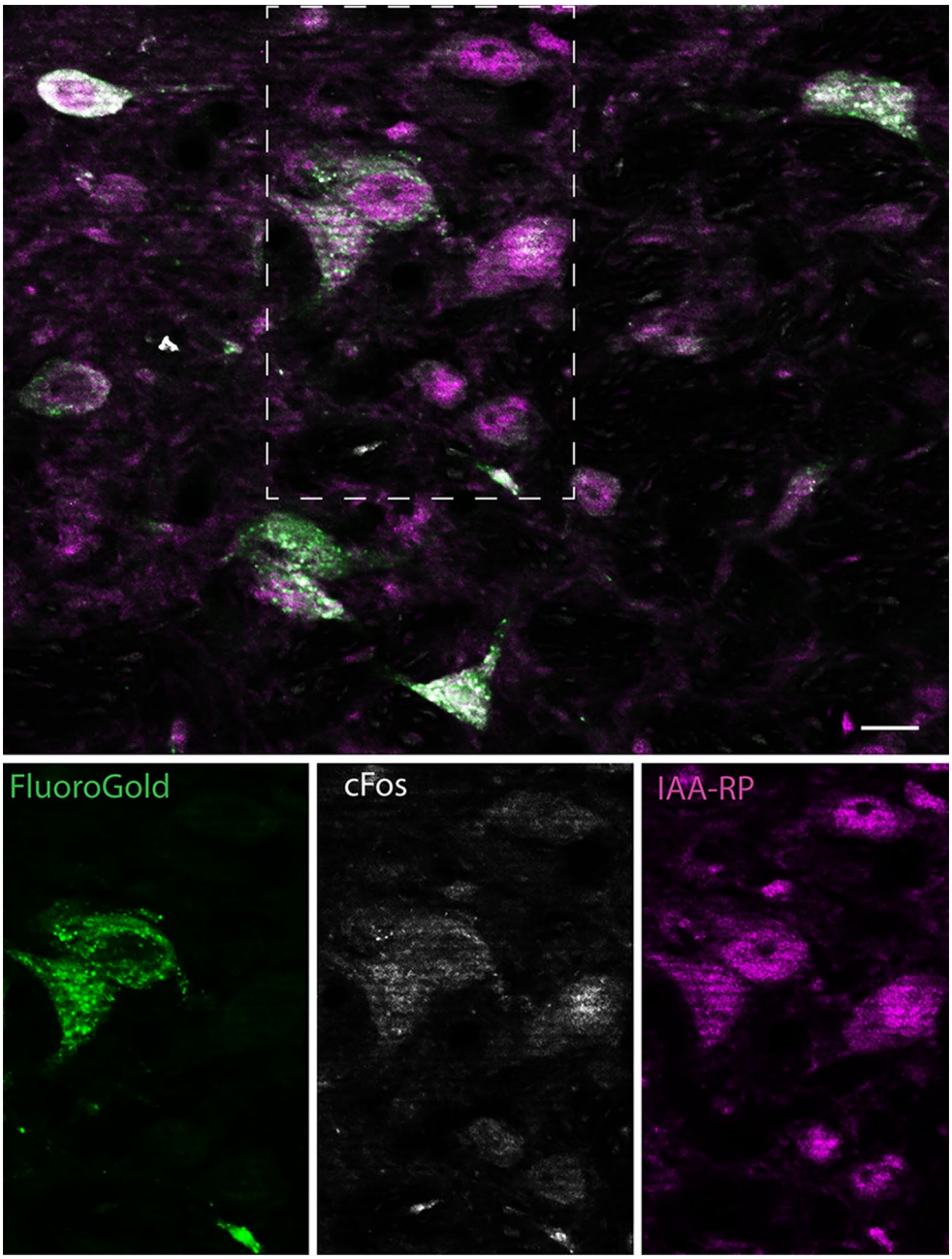

Fig. 2 Overview of vestibular neurons with direct projections to the ventrolateral medulla (FluoroGold-immunopositive), which were activated by sGVS (cFos-positive) and co-localized IAARP. *Top panel* shows a cluster of single-, double-, and triple-labeled neurons in ipsilateral SpVN from a rat with a FluoroGold injection in RVLM. The individual channel images of the *area* delineated by the *dashed rectangle* are shown in the *panels* below. These single channel images illustrate co-localization of cFos and FG in two neurons, the activation of one additional neuron that was not retrogradely filled, and the presence of IAARP in all three of those cells, as well as others in the field. *Scale bar* is 10 μm

alone (multipolar neurons, fusiform neurons, and small globular neurons) displayed triple-label co-localization. These cells were present in both SpVN and in MVN, and projected either ipsilaterally or contralaterally. It is noteworthy that some activated VSR neurons (cFos- and FluoroGold-labeled) did not appear to be glutamate immunofluorescent. Although negative immunolabeling data must be interpreted conservatively, these glutamate-*non*-immunofluorescent neurons were observed in fields in which other neural elements displayed intense glutamate

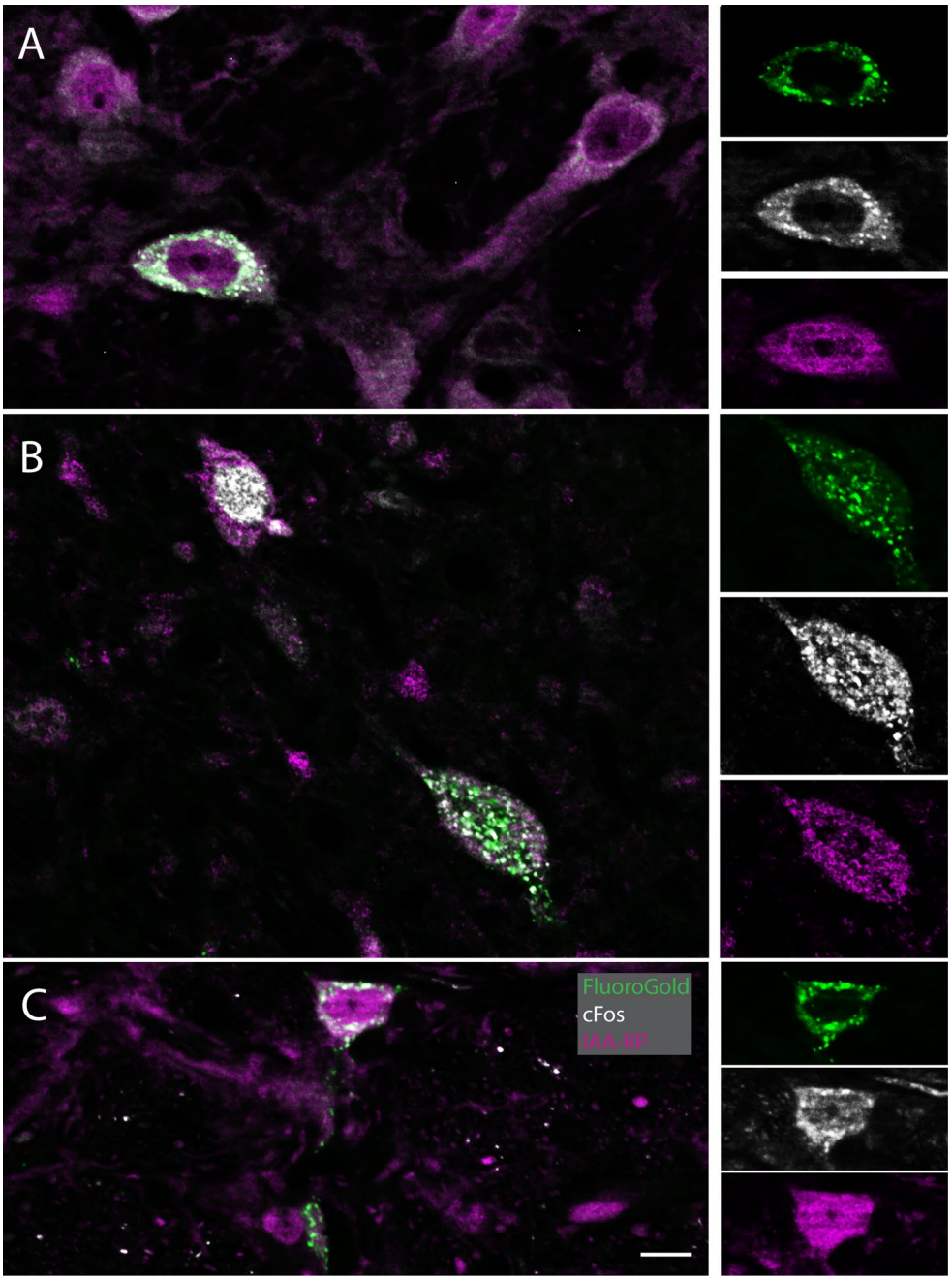

Fig. 3 IAARP is present in the cell bodies of sGVS-activated vestibular neurons with direct projections to the ventrolateral medulla. Each *large panel* (**a**–**c**) illustrates one triple-immunofluorescent vestibular neuron, as well as several double-and single-labeled cells. The *side panels* are single-channel images of the triple-labeled neurons in the *larger panels* to the *left*. For each set of *side panels*, FluoroGold label is shown at the *top*, cFos in the *center*, and IAARP at the *bottom*. **a** A multipolar neuron in SpVN with projections to contralateral CVLM. **b** A fusiform neuron in MVN that projects to ipsilateral RVLM. The smaller neuron in the *upper left quadrant* of the *panel* is cFos and IAARP-labeled, but did not contain retrograde tracer. **c** A small spherical neuron in SpVN with projections to ipsilateral RVLM. *Scale bar* is in C is 10 μm for all *large panels*. The single channel images are slightly enlarged

immunofluorescence, suggesting that antibody penetration and imaging conditions were not significant causes for the negative results. An example is shown in Fig. 5.

Of 223 FG+ and IAARP+ neurons examined in this study, 150 (67 %) were located in SpVN and 73 (33 %) were observed in caudal MVN. With the simplifying assumption that all VSR neurons project only ipsilaterally or contralaterally and that there are no bilaterally projecting VSR neurons, 151 of the 223 labeled cells (68 %) projected ipsilaterally, and 72 (32 %) projected contralaterally.

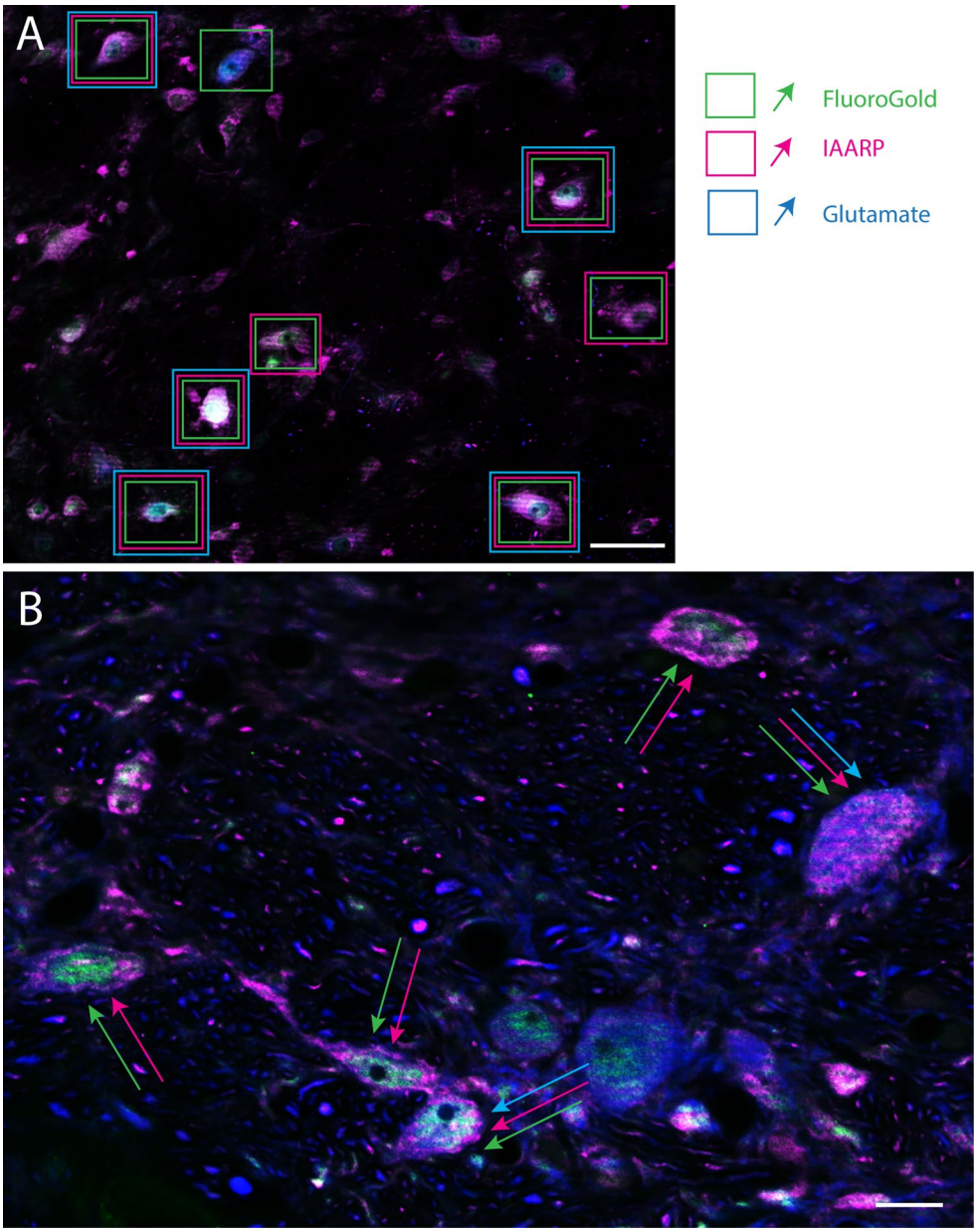

Fig. 4 Examples from two rats of the distributions of IAARP-, glutamate- and FluoroGold-immunofluorescent neurons in the caudal vestibular nuclei. **a** Low magnification image of SpVN following a tracer injection into the contralateral RVLM. Neurons surrounded by *single boxes* displayed FluoroGold tracer, but not IAARP or glutamate immunofluorescence, when the individual channels were evaluated in *gray scale*. Neurons surrounded by *two rectangles* were FluoroGold and IAARP-immunofluorescent, but did not show intense glutamate label. Cells surrounded by *three boxes* were triple-labeled. **b** A higher magnification image of SpVN following a tracer injection in the ipsilateral CVLM. Neurons identified by *two arrows* co-localized IAARP and FluoroGold, but not intense glutamate immunofluorescence; neurons indicated by *three arrows* co-localized all *three markers*. *Scale bars* 50 μm in **a**; 10 μm in **b**

Of these, 102 (46 %) IAARP+ cells were located in SpVN and projected ipsilaterally, 48 (22 %) IAARP+ cells were located in SpVN and projected contralaterally, 49 (22 %) IAARP+ cells were located in caudal MVN and projected ipsilaterally, and 24 (11 %) IAARP+ cells were located in caudal MVN and projected ipsilaterally. Of the smaller subset of these cells stained for FG, IAARP, and glutamate ($N = 89$), 52 (58 %) showed intense glutamate immunofluorescence and 37 (42 %) showed no appreciable glutamate immunolabel in microscope fields where adjacent non-VSR neurons were glutamate immunofluorescent.

To confirm the presence of IAARP in the functional VSR pathway, some sections from tracer-injected and sGVS-stimulated animals were immunolabeled for FluoroGold,

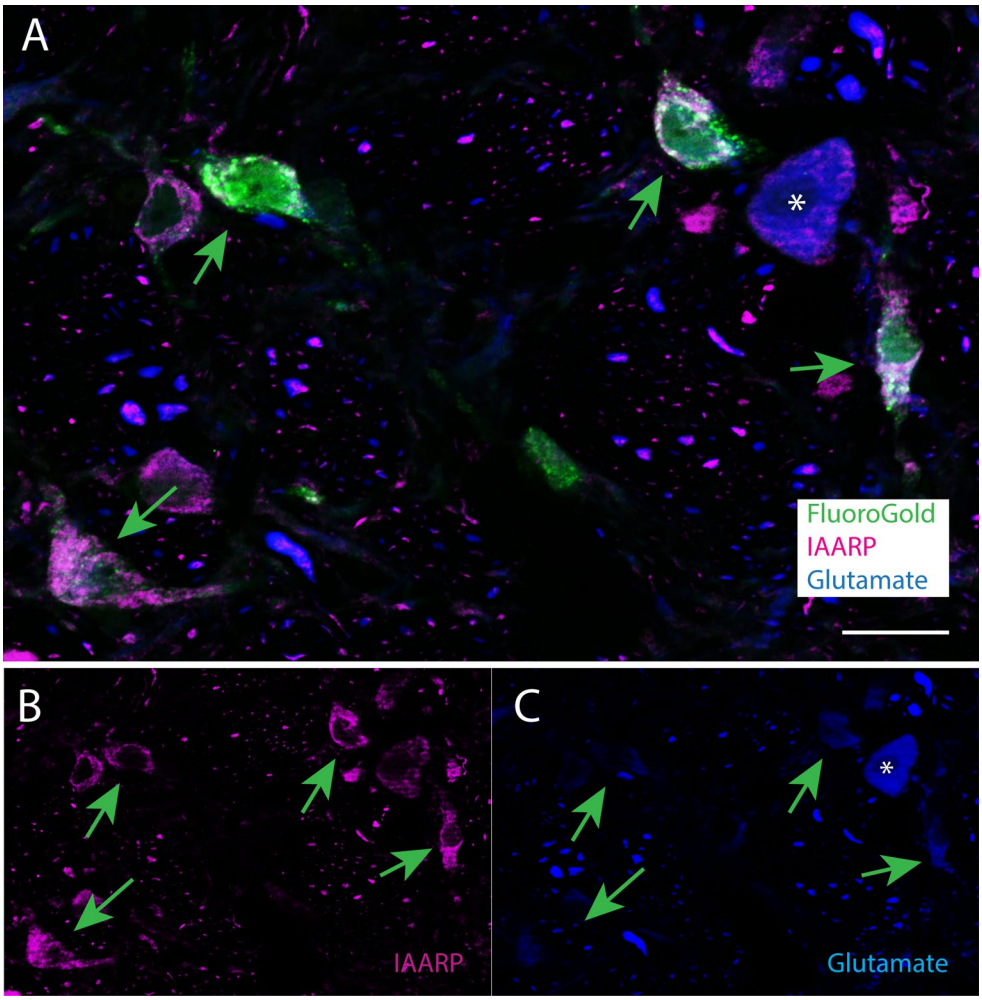

Fig. 5 Examples of IAARP- and FluoroGold-labeled vestibular neurons that are not intensely glutamate immunofluorescent. **a** The four FluoroGold-filled neurons in this image of SpVN (tracer injection in ipsilateral RVLM) are indicated by *arrows*. **b** The single channel image of IAARP in the same field. The *arrows* point to the same cells indicated in **a**. **c** The single channel image of glutamate immunofluorescence in the same field. The *arrows* point to the same cells indicated in **a** and **b**. None of the four neurons shows intense glutamate immunofluorescence, although a nearby cell body (*asterisk*) and numerous processes are labeled. *Scale bar* in **a** 20 µm

cFos, IAARP, and glutamate. Quadruple-labeled neurons of all three cytological types were observed in these sections (Fig. 6), providing strong evidence that IAARP are present in most cells of the glutamatergic limb of the VSR.

Discussion

The results of this study demonstrate that IAARP is present in vestibular nucleus neurons of the VSR pathway and frequently co-localizes in cells with intense glutamate immunofluorescence. The significance of these findings stems from the putative role of IAARP as an endogenous modulator of CNS neurons involved in blood pressure control.

CNS cells and pathways involved in blood pressure control are clinically important as drug targets for the treatment of patients with hypertension. Clonidine and several related drugs synthesized for that purpose contain an imidazole(in)e ring and are ligands at both a_2 adrenergic receptors (a_2ARs) and IRs (Bousquet et al. 1984; De Vos et al. 1994; Tolentino-Silva et al. 2000). These compounds are thought to exert their hypotensive action through inhibition of tonically active presympathetic neurons in RVLM (Karppanen 1977; Bousquet et al. 1984; Atlas 1991). The binding sites for these drugs have not been identified definitively, but three IR subtypes (I_1-, I_2- and I_3-Rs) have been distinguished pharmacologically (Eglen et al. 1998; Head and Mayorov 2006). I_1Rs are found in highest density in the brainstem, primarily in RVLM and CVLM (Moreira et al. 2004), are localized to plasma membranes, are principally neuronal, and have high affinity for the antihypertensive drugs containing a synthetic imidazoline ring

(Bousquet et al. 1984; Ernsberger et al. 1990; De Vos et al. 1994; Ernsberger and Haxhiu 1997; Wang et al. 2003; Chan et al. 2005; Nikolic and Agbaba 2012). In addition, several studies have suggested that I_1Rs are coupled to G-protein-mediated signal transduction pathways, resulting in the activation of phosphatidylcholine-sensitive phospholipase C (Separovic et al. 1997), increased phosphorylation of mitogen-activated protein kinases (MAPK1 and MAPK3) (Zhang and Abdel-Rahman 2005), and inhibition of adenylate cyclase (Greney et al. 2000). Activation of any of these second messenger mechanisms in RVLM bulbospinal neurons would result in a decrease in systemic blood pressure (for review, see Del Bello et al. 2015). I_2Rs appear to be mainly allosteric binding sites on monoamine oxidases and possibly other proteins (Remaury et al. 2000), are distributed throughout the brain, have been associated with glial cells as well as neurons (Lione et al. 1998), and are thought to be involved primarily in psychiatric disorders, analgesia, opiate withdrawal, and Parkinson's and Alzheimer's diseases (Garcia-Sevilla et al. 1990; Parini et al. 1996; Eglen et al. 1998). I_3Rs mediate insulin secretion in the pancreas (Morgan 1999) and an I_3-like binding site may also participate in blood pressure modulation (Prell et al. 2004), possibly underlying the association between hypertension and diabetes (Bousquet et al. 1984; Chan 1998; Morgan 1999).

Based on the clinical efficacy of I_1R synthetic agonists, investigators have sought to identify the endogenous ligands that bind with high affinity to these sites in brain. Four putative endogenous I_1R ligands have been proposed to date: harmane, agmatine, clonidine-displacing substance, and IAARP (reviews: Reis and Regunathan 2000; Halaris and Piletz 2007; Wu et al. 2008; Ghazaleh et al. 2015). IAARP displays high affinity binding to I_1Rs and possible also I_3Rs, producing physiological effects that are blocked by the appropriate antagonists (Prell et al. 2004). Biochemical assays and immunolabeling studies have demonstrated that IAARP is present in neurons and processes in the RVLM, and microinjection of IAARP into the RVLM region alters blood pressure in rodents (Prell et al. 2004). Results of the present study demonstrate that IAARP is localized in vestibular neurons that send direct projections to RVLM or CVLM and that are activated by vestibular stimulation. Thus, the results demonstrate that one important source of IAARP in RVLM is the VSR pathway that modulates blood pressure in response to changes in posture.

The second key finding in the present study is that IAARP- and glutamate immunofluorescence frequently co-localize within individual VSR neurons. Electrophysiological studies in rat hippocampus have examined the interaction between glutamatergic and IAARP-mediated synaptic effects. The hippocampus contains high densities of both IAARP-immunopositive neurons (Friedrich et al. 2007) and IR binding sites (Piletz et al. 2000). Using extracellular and whole-cell recordings of the Schaffer collateral-commissural pathway in rat hippocampal slices, IAARP was found to bind to IRs, resulting in the inhibition of excitatory transmission from Schaffer collaterals to CA1 pyramidal neurons. Moreover, the frequency of miniature excitatory postsynaptic currents was decreased and paired-pulse facilitation increased after bath application of IAARP, suggesting that the site of action was primarily presynaptic (Bozdagi et al. 2011). These studies demonstrate that IAARP binding to I_1Rs occurs both pre- and postsynaptically, resulting in suppression of glutamatergic neurotransmission. It is noteworthy in this context that autonomic dysregulation, including irrecoverable hypotension due to abnormalities in the hypoxia-sensitive regions of the CA1 and CA4 hippocampal fields, is speculated to play an important role in sudden unexpected death in epilepsy (Bozorgi et al. 2013) and in sudden infant death syndrome (Harper and Kinney 2010; Machaalani and Waters 2014).

Conceivably, the co-localization of IAARP- and intense glutamate immunofluorescence in VSR neurons represents an efficient configuration for up- and down-modulation of RVLM presympathetic neuronal activity. Co-release of the two neuroactive agents from single VSR pathway axons would activate fast ionotropic glutamate receptors located postsynaptically on RVLM neurons, and both pre- and postsynaptic IRs. Since the I_1R is the most likely binding target and is a G-protein-coupled receptor, this slower transmission would allow a brief burst of excitatory activity to activate RVLM bulbospinal neurons before the IAARP release would cause both presynaptic inhibition of further co-transmitter release from the axon terminal and postsynaptic inhibition of the recipient RVLM neuron.

In fact, studies assessing the effects of synthetic imidazoline agonists acting in the reticular formation on sympathetic outflow and cardiovascular function have also suggested that IRs are located presynaptically (Head 1999; Chan et al. 2005, 2007). It has been proposed that I_1Rs and a_2ARs are organized in series in the RVLM such that IRs are proximal to presynaptic sympatho-inhibitory noradrenergic terminals (Molderings and Göthert 1999), and α_2ARs lie more distally, possibly as somatic autoreceptors (Head 1999; Chan et al. 2005). The present results suggest further complexity to the receptor interplay in RVLM.

This complexity is underscored by the observation that some VSR pathway neurons appear to utilize GABA (Holstein et al. 2016), rather than an excitatory glutamatergic neurotransmitter. It is possible that some of the non-glutamate immunofluorescent and IAARP-positive VSR neurons observed in the present study are part of the GABAergic limb of the VSR, which is primarily directed to CVLM. In

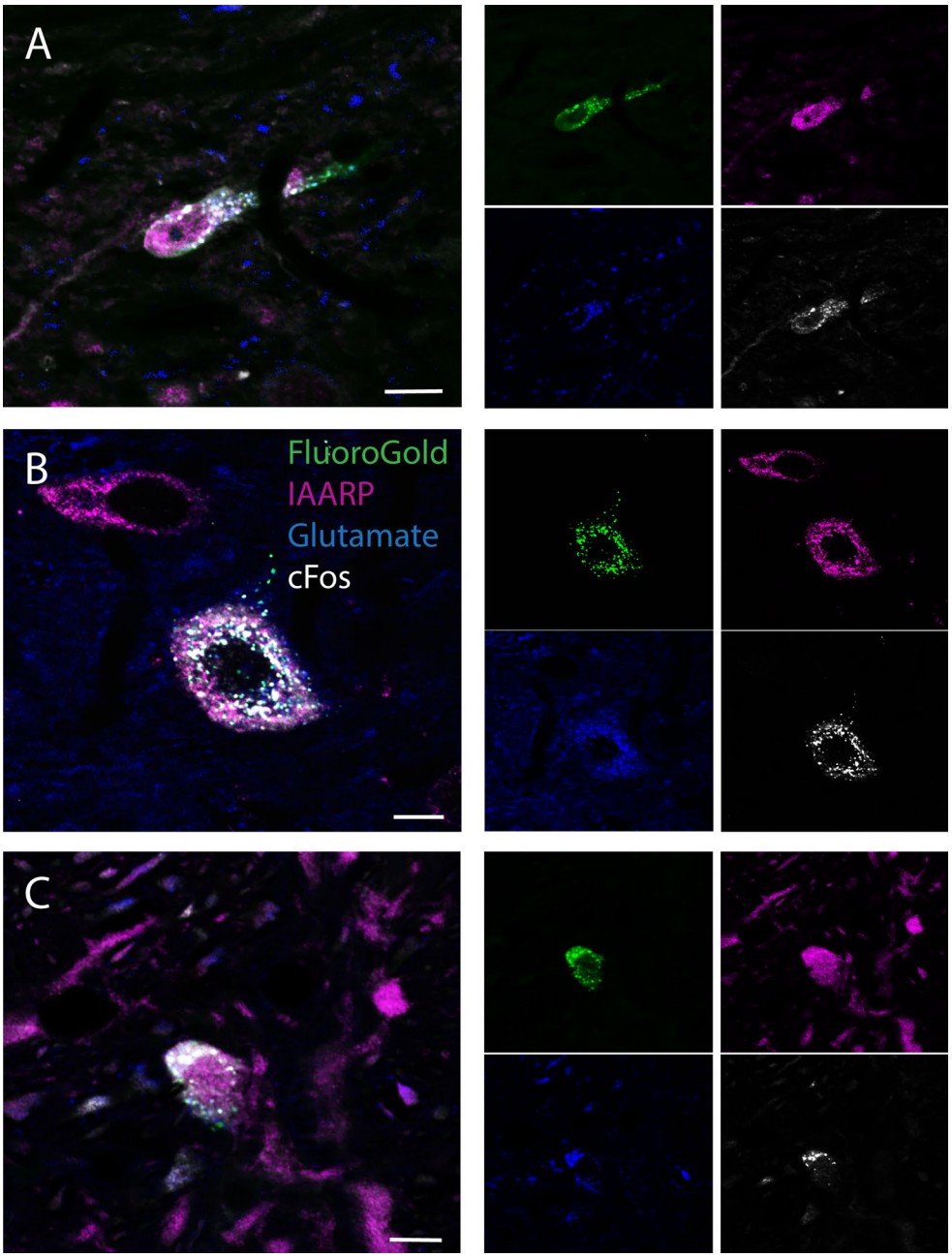

Fig. 6 Co-localization of IAARP and glutamate in sGVS-activated (cFos-positive) and retrogradely filled (FluoroGold-positive) vestibular neurons. The *larger panels* (**a**–**c**) illustrate quadruple-labeled neurons of three cytologic types. The *side panels* are the single channel images of the labeled neurons in the *larger panels* to the *left*. For each set of *side panels*, FluoroGold tracer is shown in the *upper left panel*, IAARP immunofluorescence is shown in the *upper right panel*, glutamate immunofluorescence is shown in the *lower left panel,* and cFos immunofluorescence is shown in the *lower right panel*. **a** A fusiform neuron in MVN after a tracer injection in the ipsilateral CVLM. **b** A large multipolar neuron in MVN after a tracer injection in the ipsilateral RVLM. **c** A small spherical neuron in SpVN after a tracer injection in ipsilateral CVLM. *Scale bars* in all *three panels*: 10 μm

this context, it is interesting to note that an electrophysiological study in acute slices of rat striatum provided evidence that presynaptic I_1Rs are involved in the inhibition of $GABA_A$-mediated inhibitory postsynaptic currents by the imidazoline drug moxonidine (Tanabe et al. 2006). In fact, we have presented preliminary data showing that IAARP has similar inhibitory effects on inhibitory postsynaptic currents in striatal slices (Artis et al. 2007). Postsynaptic effects are also likely to contribute to shaping the inhibitory synaptic response to IAARP obtained in the acute hippocampal slices, and additional studies will be necessary to identify the mechanisms underlying these effects in the RVLM.

Acknowledgments The authors are grateful to Dr. Sergei Yakushin for assistance with the sGVS stimulation, Dr. Ewa Kukielka for technical assistance, and Dr. George Prell for helpful discussions concerning IAARP. The research was supported by NIH Grant DC008846.

Author contributions All authors approved the final version of this article. Experiments were conceived and designed by GH, GM, and VF. GM performed the tracer injections, sGVS stimulation, and immunolabeling studies; GH performed the microscopy, image processing, and data analysis. GH prepared the figures, and all authors contributed to the manuscript preparation.

References

Artis AS, Bozdagi O, Prell GP, Holstein GR, Huntley GW, Martinelli GP (2007) Endogenous imidazol(in)e receptor ligand modulates corticostriatal synaptic transmission. Soc Neurosci Abstr 893.2

Atlas D (1991) Clonidine-displacing substance (CDS) and its putative imidazoline receptor. New leads for further divergence of a_2-adrenergic receptor activity. Biochem Pharmacol 41:1541–1549

Bourassa EA, Sved AF, Speth RC (2009) Angiotensin modulation of rostral ventrolateral medulla (RVLM) in cardiovascular regulation. Mol Cell Endocrinol 302:167–175

Bousquet P, Feldman J, Schwartz J (1984) Central cardiovascular effects of α-adrenergic drugs: difference between catecholamines and imidazolines. J Pharmacol Exp Ther 230:232–236

Bozdagi O, Martinelli GP, Prell GD, Friedrich VLJ, Huntley GW, Holstein GR (2011) Imidazoleacetic acid-ribotide induces depression of synaptic responses in hippocampus through activation of Imidazoline receptors. J Neurophysiol 105:1266–1275

Bozorgi A, Chung S, Kaffashi F et al (2013) Significant postictal hypotension: expanding the spectrum of seizure-induced autonomic dysregulation. Epilepsia 54:e127–e130

Card JP, Sved JC, Craig B, Raizada M, Vazquez J, Sved AF (2006) Efferent projections of rat rostroventrolateral medulla C1 catecholamine neurons: implications for the central control of cardiovascular regulation. J Comp Neurol 499:840–859

Chan SL (1998) Clonidine-displacing substance and its putative role in control of insulin secretion: a minireivew. Gen Pharmacol 31:525–529

Chan CKS, Burke SL, Zhu H, Piletz JE, Head GA (2005) Imidazoline receptors associated with noradrenergic terminals in the rostral ventrolateral medulla mediate the hypotensive responses of moxonidine but not clonidine. Neuroscience 132:991–1007

Chan CK, Burke SL, Head GA (2007) Contribution of imidazoline receptors and alpha2-adrenoceptors in the rostral ventrolateral medulla to sympathetic baroreflex inhibition by systemic rilmenidine. J Hypertens 25:147–155

Cohen B, Martinelli GP, Raphan T, Schaffner A, Xiang Y, Holstein GR, Yakushin SB (2013) The vasovagal response of the rat: its relation to the vestibulosympathetic reflex and to Mayer waves. FASEB J 27:2564–2572

De Vos H, Bricca G, DeKeyser J, DeBacker J-P, Bousquet P, Vauquelin G (1994) Imidazoline receptors, non-adreneergic idazoxan binding sites and a_2-adrenoceptors in the human central nervous system. Neuroscience 59:589–598

Del Bello F, Bargelli V, Cifani C et al (2015) Antagonism/agonism modulation of build novel antihypertensives selectively triggering I1-imidazoline receptor activation. ACS Med Chem Lett 6:496–501

Deuchars SA, Morrison SF, Gilbey MP (1995) Medullary-evoked EPSPs in neonatal rat sympathetic preganglionic neurones in vitro. J Physiol 487:453–463

Eglen RM, Hudson AL, Kendall DA, Nutt DJ, Morgan NG, Wilson VG, Dillon MP (1998) Seeing through a glass darkly: casting light on the imidazoline "I" sites. Trends Pharmacol Sci 19:381–390

Ernsberger P, Haxhiu MA (1997) The I1-imidazoline-binding site is a functional receptor mediating vasodepression via the ventral medulla. Am J Physiol 273:R1572–R1579

Ernsberger P, Feinland G, Meeley MP, Reis DJ (1990) Characterization and visualization of clonidine-sensitive imidazole sites in rat kidney which recognize clonidine-displacing substance. Am J Hypertens 3:90–97

Ernsberger P, Elliott HL, Weimann H-J et al (1993) Moxonidine: a second-generation central antihypertensive agent. Cardiovasc Drug Rev 11:411–431

Friedrich VLJ, Martinelli GP, Prell GD, Holstein GR (2007) Distribution and cellular localization of imidazoleacetic acid-ribotide, an endogenous ligand at imidazol(in)e and adrenergic receptors, in rat brain. J Chem Neuroanat 33:53–64

Garcia-Sevilla JA, Escriba PV, Guimon J (1990) Imidazoline receptors and human brain disorders. Ann N Y Acad Sci 881:392–409

Ghazaleh HA, Tyacke RJ, Hudson AL (2015) Borne identity: leading endogenous suspects at imidaoline binding sites. J Neurol Neurosci 6:11

Goodchild AK, Moon EA (2009) Maps of cardiovascular and respiratory regions of rat ventral medulla: focus on the caudal medulla. J Chem Neuroanat 38:209–221

Greney U, Ronde P, Magnier C et al (2000) Coupling of I1 imidazoline receptors to the cAMP pathway: studies with a highly selective ligand, Benazoline. Mol Pharmacol 57:1142–1151

Halaris A, Piletz J (2007) Agmatine: metabolic pathway and spectrum of activity in brain. CNS Drugs 21:885–900

Harper RM, Kinney HC (2010) Potential mechanisms of failure in the sudden infant death syndrome. Curr Pediatr Rev 6:39–47. doi:10.2174/157339610791317214

Head GA (1999) Central imidazoline- and *a*2-receptors involved in the cardiovascular actions of centrally acting antihypertensive agents. Ann N Y Acad Sci 881:279–286

Head GA, Mayorov DN (2006) Imidazoline receptors, novel agents and therapeutic potential. Cardiovasc Hematol Agents Med Chem 4:17–32

Holstein GR, Martinelli GP, Henderson SC, Friedrich VLJ, Rabbitt RD, Highstein SM (2004) Gamma-aminobutyric acid is present in a spatially discrete subpopulation of hair cells in the crista ampullaris of the toadfish, Opsanus tau. J Comp Neurol 471:1–10

Holstein GR, Friedrich VLJ, Kang T, Kukielka E, Martinelli GP (2011a) Direct projections from the caudal vestibular nuclei to the ventrolateral medulla in the rat. Neuroscience 175:104–117

Holstein GR, Martinelli GP, Friedrich VLJ (2011b) Anatomical observations of the caudal vestibulo-sympathetic pathway. J Vestib Res 21:49–62

Holstein GR, Friedrich VLJ, Martinelli GP, Ogorodnikov D, Yakushin SB, Cohen B (2012) Fos expression in neurons of the rat vestibulo-autonomic pathway activated by sinusoidal galvanic vestibular stimulation. Front Neurol 3:1–12

Holstein GR, Friedrich VLJ, Martinelli GP (2014) Projection neurons of the vestibulo-sympathetic reflex pathway. J Comp Neurol 522:2053–2074

Holstein GR, Friedrich VL, Martinelli GP (2016) Glutamate and GABA in vestibulo-sympathetic pathway neurons. Front Neuroanat. doi:10.3389/fnana.2016.00007

Karppanen H (1977) Comparison of central hypotensive effects of clonidine and imidazole acetic acid. Acta Pharmacol Toxicol 41:20

Lione LA, Nutt DJ, Hudson AL (1998) Characterisation and localisation of [3H] 2-(2-benzofuranyl)-2-imidazoline binding in rat

brain: a selective ligand for imidazoline I 2 receptors. Eur J Pharmacol 353:123–135

Lipski J, Kanjhan R, Kruszewska B, Smith M (1995) Barosensitive neurons in the rostral ventrolateral medulla of the rat in vivo: morphological properties and relationship to C1 adrenergic neurons. Neuroscience 69:601–618

Machaalani R, Waters KA (2014) Neurochemical abnormalities in the brainstem of the Sudden Infant Death Syndrome (SIDS). Paediatric Respir Rev 15:293–300

Martinelli GP, Friedrich VLJ, Prell GD, Holstein GR (2007) Vestibular neurons in the rat contain imidazoleacetic acid-ribotide, a putative neurotransmitter involved in blood pressure regulation. J Comp Neurol 501:568–581

Molderings GJ, Göthert M (1999) Imidazoline binding sites and receptors in cardiovascular tissue. Gen Pharmacol 32:17–22

Moreira TS, Takakura AC, Menani JV, Sato MA, Colombari E (2004) Central blockade of nitric oxide synthesis reduces moxonidine-induced hypotension. Br J Pharmacol 142:765–771

Morgan NG (1999) Imidazoline receptors: new targets for anti-hyperglycemic drugs. Exp Opin Invest Drugs 8:575–584

Morrison SF (2003) Glutamate transmission in the rostral ventrolateral medullary sympathetic premotor pathway. Cell Mol Neurobiol 23:761–772

Nikolic K, Agbaba D (2012) Imidazoline antihypertensive drugs: selective I1-imidazoline receptor activation. Cardiovasc Ther 30:209–216

Parini A, Moudanos CG, Pizzinat N, Lanier SM (1996) The elusive family of imidazoline binding sites. Trends Pharmacol Sci 17:13–16

Paxinos G, Watson C (2005) The rat brain in stereotaxic coordinates. Academic Press, London

Paxinos G, Watson C (2009) The rat brain in stereotaxic coordinates. Academic Press, London

Piletz JE, Ivanov TR, Sharp JD et al (2000) Imidazoline receptor antisera-selected (IRAS) cDNA: cloning and characterization. DNA Cell Biol 19:319–329

Prell GD, Martinelli GP, Holstein GR et al (2004) Imidazoleacetic acid-ribotide: an endogenous ligand that stimulates imidazol(in)e receptors. Proc Natl Acad Sci U S A 101:13677–13682

Raju DV, Smith Y (2006) Anterograde axonal tract tracing. Curr Protoc Neurosci 1:1–14

Regunathan S, Reis DJ (1996) Imidazoline receptors and their endogenous ligands. Ann Rev Pharmacol Toxicol 36:511–544

Reis DJ, Regunathan S (2000) Is agmatine a novel neurotransmitter in brain? Trends in Pharmacol. Science 21:187–193

Remaury A, Raddatz R, Ordener C et al (2000) Analysis of the pharmacological and molecular heterogeneity of I(2)-imidazoline-binding proteins using monoamine oxidase-deficient mouse models. Mol Pharmacol 58:1085–1090

Ruggiero DA, Cravo SL, Golanov E, Gomez R, Anwar M, Reis DJ (1994) Adrenergic and non-adrenergic spinal projections of a cardiovascular-active pressor area of medulla oblongata: quantitative topographic analysis. Brain Res 663:107–120

Schofield BR (2008) Retrograde axonal tracing with fluorescent markers. Curr Protoc Neurosci 43:1–17

Schreihofer AM, Guyenet PG (1997) Identification of C1 presympathetic neurons in rat rostral ventrolateral medulla by juxtacellular labeling in vivo. J Comp Neurol 387:524–536

Separovic D, Kester M, Haxhiu MA, Ernsberger P (1997) Activation of phosphatidylcholine-selective phospholipase C by I1-imidazoline receptors in PC12 cells and rostral ventrolateral medulla. Brain Res 749:335–339

Stornetta RL (2009) Neurochemistry of bulbospinal presympathetic neurons of the medulla oblongata. J Chem Neuroanat 38:222–230

Tanabe M, Kino Y, Honda M, Ono H (2006) Presynaptic I1-Imidazoline receptors reduce GABAergic synaptic transmission in striatal medium spiny neurons. J Neurosci 26:1795–1802

Tolentino-Silva FP, Haxhiu MA, Waldbaum S, Dreshay IA, Ernsberger P (2000) α2-Adrenergic receptors are not required for central antihypertensive action of moxonidine in mice. Brain Res 862:26–35

Vidal PP, Cullen KE, Curthoys IS et al (2015) The Vestibular System. In: Paxinos G, Watson C (eds) The rat nervous system, 4th edn. Elsevier Academic Press, London, pp 805–864

Wang W-Z, Yuan W-J, Ren A-J, Pan Y-X, Tang C-S, Su D-F (2003) Role of I1-imidazoline receptors within the caudal ventrolateral medulla in cardiovascular responsees to clonidine in rats. J Cardiovasc Pharmacol 42:1–9

Wu N, Su R-B, Li J (2008) Agmatine and imidazoline receptors: their role in opioid analgesia, tolerance and dependence. Cell Mol Neurobiol 28:629–641

Yates BJ, Bolton PS, Macefield VG (2014) Vestibulo-sympathetic responses. Compr Physiol 4:851–887

Zhang J, Abdel-Rahman AA (2005) Mitogen-activated protein kinase phosphorylation in the rostral ventrolateral medulla plays a key role in imidazoline (I1)-receptor-mediated hypotension. J Pharmacol Exp Ther 314:945–952